Journal of the Korean Electrochemical Society
Vol. 29, No. 3, 2026, 47-59
https://doi.org/10.5229/JKES.2026.29.3.47

Research Paper
pISSN 1229-1935
eISSN 2288-9000

FTO에서 전기합성된 PPy의 시트 저항을 줄이기 위한 조정 가능한 첨가제로서의 물

Water as a Tunable Additive for Reducing the Sheet Resistance of PPy Electrosynthesized on FTO

Gregorio Villasana-Ponce, Luis F. Cisneros-Sinencio*, and Ulises Páramo-García

División de Estudios de Posgrado e Investigación, Instituto Tecnológico de Cd. Madero, Juventino Rosas y Jesús Ureta S/N, Col. Los Mangos, 89440 Cd. Madero, Tamps., MEXICO

(Received April 24, 2026 : Revised May 16, 2026 : Accepted May 30, 2026)

Graphical abstract

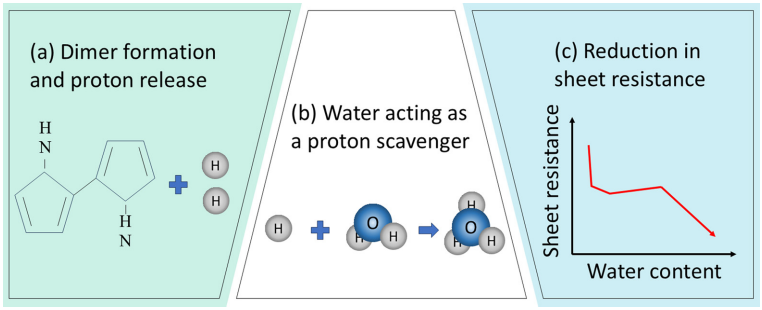

초 록

비수용성 전기중합에서 미량의 수분은 흔히 오염물질로 간주되지만, 전도성 고분자의 전자적 특성에 지대한 영향을 미칠 수 있다. 본 연구에서는 물이 불소 도핑 산화주석(FTO) 기판 상에서 폴리피롤(PPy)의 전기합성 과정에서 성능 향상 첨가제로 작용함을 보여준다. 아세토니트릴/$LiClO_4$ 전해액에서 수분 농도를 0.0%에서 10.0%(wt)까지 변화시켰을 때, 면저항은 70% 이상 감소(433 Ω/sq에서 131 Ω/sq로)하는 반면, 부피전도도(σ)는 수분 함량이 0.3%일 때 최대값인 120 S/cm를 나타낸 후 감소하는 경향을 보이며, 이러한 전기적 특성들 사이에 발산적인 관계가 있음을 확인했다. 이는 기판에 평행하게 배열된 공액 골격과 π-π 스태킹을 형성하는 주된 에지온(edge-on) 구조로 설명할 수 있으며, 이로 인해 평면 내 전하 이동이 용이해지는 반면, 부피 전도는 측면 간격을 가로지르는 기둥 간 전하 이동에 의해 제한된다. 측정 결과, 물은 양성자 제거제 역할을 하여 산 촉매에 의한 공액 구조 파괴 결함 형성을 억제하는 것으로 나타났다. 이러한 결과는 물이 PPy 필름의 전기적 성능을 조절하는 간단한 분자 도구임을 입증한다.

Abstract : Trace water content in non-aqueous electropolymerization media is often regarded as a contaminant, yet its deliberate incorporation can profoundly influence the electronic properties of conducting polymers. In this work, we demonstrate that water functions as a tunable performance-enhancing additive in the electrosynthesis of polypyrrole (PPy) on fluorine-doped tin-oxide (FTO) substrates. By systematically varying water concentration from 0.0 to 10.0 wt.%

*E-mail: fortino.cs@cdmadero.tecnm.mx

in an acetonitrile/$LiClO_4$ electrolyte, we achieve a > 70% reduction in sheet resistance (from 433 to 131 Ω/sq), while bulk conductivity (σ) exhibits a maximum of 120 S/cm at 0.3 wt.% water content followed by a decreasing trend, revealing a divergent relationship between these electrical properties. This divergence can be explained by a predominant edge-on texture that aligns conjugated backbones and π-π stacking parallel to the substrate, facilitating in-plane transport while volumetric conduction remains constrained by intercolumnar charge transfer across lateral spacing. Chronoamperometry (CA), FTIR spectroscopy, and four-point probe measurements reveal that water enhances sheet resistance by acting as a proton scavenger that suppresses acid-catalyzed formation of conjugation-disrupting defects. These findings establish water as a simple, cost-effective, and highly effective molecular tool for tuning the electrical performance of PPy films, with direct implications for applications such as gas sensors and solar cells.

Keywords : Polypyrrole, Polymerization additive, Electropolymerization, Sheet resistance, FTO substrate, 3D Progressive Nucleation, Proton scavenger

1. Introduction

Electrical conduction is the hallmark feature that distinguishes conducting polymers from conventional organic polymers. Unlike typical polymers, these materials conduct electricity via delocalized π-electrons along a conjugated backbone, a feature that can be enhanced by chemical or electrochemical doping to achieve conductivities that rival those of metals.[1,2] This characteristic has positioned conducting polymers as indispensable components in next-generation devices such as supercapacitors, rechargeable batteries, and sensors.[1–4] While their optical, magnetic, and mechanical properties are also valuable, it is their ability to conduct electricity that fundamentally enables these applications and drives research to optimize their performance through molecular design and control of synthesis.[4,5]

Polypyrrole (PPy) is among the most widely investigated conducting polymers, valued for its highly tunable electronic properties.[6–8] In its undoped state, PPy is essentially insulating; however, its electrical conductivity, far from being intrinsic, can be enhanced by several orders of magnitude through careful control of synthesis parameters.[9,10] It can be synthesized either by chemical oxidative polymerization, in which an external oxidant initiates chain growth in solution, or by electrochemical polymerization, in which the chemical oxidant is replaced by an applied potential at the electrode surface.[5,11,12]

In chemically synthesized PPy, the choice of dopant plays a decisive role in determining the efficiency of charge transport.[10,13] Beyond dopant selection, reaction conditions such as polymerization temperature significantly affect the resulting conductivity, as PPy conductivity increases at lower temperatures.[14] The oxidant-to-monomer ratio is another critical variable; an optimal balance is required to maximize polymer yield and conjugation length without inducing over-oxidation or side reactions.[8,15–18] Likewise, the chemical identity of the oxidant, such as iron (III) chloride, directly affects polymerization kinetics and film quality, thereby shaping the final electrical performance.[19–21] Together, these parameters illustrate that PPy's electronic properties are not predetermined but can be rationally engineered through synthesis design.

In the context of electrochemical polymerization, despite extensive optimization of classical synthesis parameters, such as dopant ions, monomer concentration, and electrolyte, the role of additives in the electrolyte has historically been overlooked.[11] Water exemplifies this oversight and presents an apparent paradox: Yan et al. showed that when used as a solvent, water yields low-conductivity PPy due to its high donor number and strong nucleophilic interference with radical intermediates.[22] In contrast, Zhou and Heinze established that when employed as an additive in aprotic media such as acetonitrile (ACN), water acts not as a contaminant but as a proton scavenger that suppresses acid-catalyzed side reactions. Their work revealed that controlled incorporation of water in such systems can significantly improve PPy electropolymerization, highlighting its role in determining electronic performance.[23]

In this study, we demonstrate that the "water effect" is a tunable design parameter for engineering the electronic performance of PPy. By varying water content from 0.0 to 10.0 wt.% in an acetonitrile/$LiClO_4$ electrolyte, we achieve a progressive enhancement in in-plane charge transport, culminating in a > 70% reduction in sheet resistance at the highest concentration, while bulk conductivity reaches a maximum at 0.3 wt.% water content and subsequently declines, demonstrating a non-parallel response between these transport metrics. Using chronoamperometry, FTIR spectroscopy, and four-point probe measurements coupled with nucleation and growth kinetics on PPy/FTO films, we establish that water is a simple, cheap, and effective additive for tailoring the electronic properties of PPy films. These results provide a practical and sustainable strategy for optimizing conductive PPy films in next-generation sensing, energy, and optoelectronic devices.

2. Materials and methods

2.1. Electrode preparation and electropolymerization of PPy

Fluorine-doped tin oxide (FTO) glass substrates (Sigma-Aldrich, SnO_2:F, purity of at least 99%) were used as working electrodes (WE). Prior to deposition, FTO slides (1.0 cm × 2.0 cm) were ultrasonically cleaned for 10 min each in acetone, ethanol, and deionized water, and then dried. The geometric area of the FTO working electrode exposed to the electrolyte was carefully masked to 1.0 cm^2. The electrosynthesis of PPy was performed via chronoamperometry at a constant potential of +0.8 V vs. Ag/AgCl (3 M KCl, Metrohm) using an Autolab PGSTAT302N potentiostat/galvanostat in a standard three-electrode cell. A stainless steel plate served as the counter electrode.

The polymerization electrolyte consisted of pyrrole monomer (Sigma-Aldrich, purity of at least 98%, 0.25 M) dissolved in acetonitrile (Sigma-Aldrich, purity of at least 99.9%), with lithium perchlorate ($LiClO_4$, Sigma-Aldrich, purity of at least 95%, 0.5 M) added as the supporting electrolyte. To evaluate the effect of water content on the PPy films, variable volumes of deionized water (0–2000 μL, corresponding to 0.0–10.0 wt.%) were added to the 20 mL electrolyte solution under stirring immediately before deposition. Each experiment was conducted for 210 s, and after deposition, the PPy-coated FTO electrodes were rinsed gently with acetonitrile and dried under ambient conditions.

2.2. PPy films characterization

The temporal evolution of current during polymerization was analyzed to determine the mechanism of nucleation and growth according to the theoretical model proposed by Scharifker and Hills.[24–28] By fitting the experimental chronoamperometric curves to the dimensionless current-time relationships for instantaneous or progressive nucleation under diffusion-controlled conditions. Following electrochemical analysis, the sheet resistance (Rs) of the deposited PPy films was evaluated using the four-point probe technique with a Signatone S301 system (Signatone, USA), equipped with a manual probe head and digital multimeter (Keithley 2410, USA). Measurements were performed at room temperature on multiple points across each sample to ensure reproducibility. To gain deeper insight into the intrinsic electrical properties of the PPy films, the bulk conductivity (σ) was calculated from the Rs and film thickness. The film thickness was estimated from the electrodeposition charge density via Faraday's law, assuming 100% faradaic efficiency and uniform growth.[29,30] Although this assumption is idealized, it provides a consistent comparative framework. Finally, to correlate film performance with molecular structure, the synthesized polypyrrole films were characterized using attenuated total reflectance Fourier transform infrared spectroscopy (FTIR). Spectra were recorded on a PerkinElmer Spectrum 100 spectrometer equipped with a diamond ATR crystal. Measurements were performed directly on the surface of the PPy/FTO electrodes without any sample preparation, over the wavenumber range of 4000–400 cm^{-1}, with a resolution of 4 cm^{-1} and 32 scans per spectrum. To facilitate quantitative and comparative analysis across the synthesized films, the transmittance data were converted to absorbance. This conversion is fundamental in infrared spectroscopy, as absorbance exhibits a direct linear relation-

ship with the concentration of the absorbing functional group, in accordance with the Beer–Lambert law, thereby enabling more accurate and meaningful comparisons between samples.[31,32] The conversion allowed the absorption bands to be visualized as positive peaks, enhancing clarity for identifying and comparing the intensity of characteristic signals.

3. Results and discussion

3.1 Interfacial proton accumulation during PPy electropolymerization

The influence of water concentration on the electrochemical behavior during pyrrole polymerization is clearly illustrated in Fig. 1, which shows chronoamperometric curves for electrolytes containing 0.0-10.0 wt.% water. All curves exhibit the characteristic behavior of pyrrole electrochemical polymerization, with an initial current peak associated with monomer oxidation and film nucleation, followed by a stabilization phase reflecting the growth of the polymeric film.[12,33–35] However, it is evident that the current magnitude is directly proportional to the water percentage: whereas the red curve corresponding to 0.0 wt.% water displays the lowest and most stable current, indicative of a slow reaction likely limited by low ionic mobility, the orange curve with 10.0 wt.% water reaches significantly higher current values, featuring a more pronounced initial peak and a subsequent rising trend, suggesting enhanced electronic conductivity. This systematic variation in the electrochemical response confirms that water acts as a key modulator of PPy deposition kinetics, substantially increasing both the polymerization rate and the electrochemical process efficiency on FTO.

The influence of water can be understood in terms of the polymerization mechanism, in which the generation and removal of protons (H^+) are critical. During pyrrole electropolymerization, each propagation step involves the electrochemical oxidation of monomers or growing oligomers, followed by α-α coupling and deprotonation to restore aromaticity and π-conjugation in the polymer backbone. This final step releases protons directly at the electrode–solution interface.[6,9,36,37]

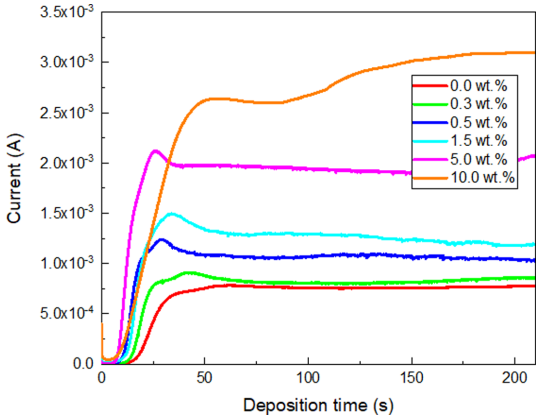

Fig. 1. Effect of water content on the chronoamperometric response during electropolymerization of PPy/FTO.

At the initial instant (t = 0), the proton concentration throughout the bulk solution is homogeneous and, in non-aqueous systems such as acetonitrile, can be extremely low. However, upon application of an anodic potential and initiation of polymerization (t > 0), protons are generated at the electrode surface, creating a concentration gradient. This gradient drives the diffusion of H^+ ions from the interface into the bulk solution, establishing a proton diffusion layer whose thickness (δH^+) increases with deposition time (Fig. 2).[38]

This accumulation of H^+ creates a highly acidic microenvironment that promotes an undesired secondary reaction pathway. While the ideal conductive PPy forms through α-α coupling, preserving a conjugated backbone, the proton concentration favors competing β-coupling pathways.[9,34,39] When pyrrole monomers are joined by α-α coupling, a linear and planar backbone with extended π-conjugation is formed. This structural continuity lowers the energetic barrier for electrochemical oxidation, effectively promoting extended charge delocalization along the π-conjugated backbone. Consequently, α-α coupling facilitates the efficient generation of a high density of polarons and bipolarons, while simultaneously enhancing intrachain charge-carrier mobility along the conjugated polymer backbones. In contrast, β-coupling introduces structural kinks that disrupt backbone planarity and break the continuous π-orbital overlap. This effectively shortens

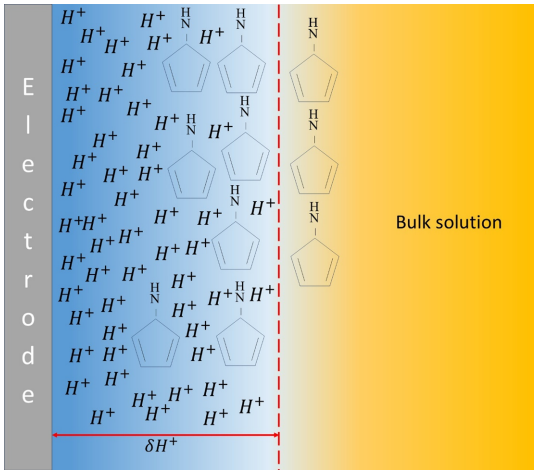

Fig. 2. Schematic representation of proton accumulation at the electrode–solution interface during pyrrole electropolymerization, leading to localized acidification and potential disruption of the polymerization mechanism.

the conjugation length, fragmenting the polymer into isolated conductive segments separated by energetic barriers. Consequently, charge transport can no longer proceed via efficient intrachain delocalization but must rely on interchain hopping, a significantly less efficient mechanism that reduces both polaron mobility and the effective density of mobile charge carriers.[1,2,33)]

To prevent the local accumulation of protons that promotes the formation of defective structures in PPy, it is essential to incorporate an additive capable of reducing the H^+ concentration at the electrode–solution interface. The ability of a species to scavenge these protons depends on its basicity, which reflects its molecular capacity to accept protons.[40)] Pyrrole can act as a base, but its ability to accept a proton is limited, as reflected by its pK_a value of 3.4. This weak basicity arises because the nitrogen lone pair is delocalized into the aromatic π-system of the five-membered ring, where it plays a crucial role in maintaining aromaticity. Consequently, this electron pair is unavailable for bonding with a proton without disrupting the ring's resonance stabilization. Nevertheless, under conditions of high proton concentration, pyrrole can undergo protonation, resulting in the loss of aromaticity.[41,42)] In contrast, water possesses a localized lone pair on oxygen that is readily available for proton acceptance. The conjugate acid of water is the hydronium ion (H_3O^+), which has a pK_a of –1.7. This difference demonstrates that water is a stronger base than neutral pyrrole. This higher basicity enables water to effectively compete for the protons released during electropolymerization, thereby mitigating local acidification at the electrode interface.[41,43)] This water-buffering action is crucial for promoting the desired polymerization pathway and for obtaining a well-conjugated, highly conductive polypyrrole film.[9)]

3.2 FTIR characterization of PPy films.

All spectra shown in Fig. 3 exhibit the fundamental vibrational bands that confirm the presence of the PPy skeleton. The broad, strong absorption band centered at 3338 cm^{-1} is attributed to the overlap of different functional-group bands, including the N–H stretching vibration of the pyrrole rings and the O–H stretching vibration of residual or incorporated water, suggesting the likely presence of hydrogen-bonding interactions within the polymer matrix.[44–47)] The bands at 2956 cm^{-1} and 2925 cm^{-1} correspond to asymmetric and symmetric C–H stretching vibrations of the pyrrole ring. The peak at 1630 cm^{-1} is assigned to the combined C=C and C–C skeletal stretching vibrations of the aromatic pyrrole ring, a key indicator of π-conjugation extension. The absorption band at 1249 cm^{-1} is characteristic of C–N stretching vibrations, confirming the

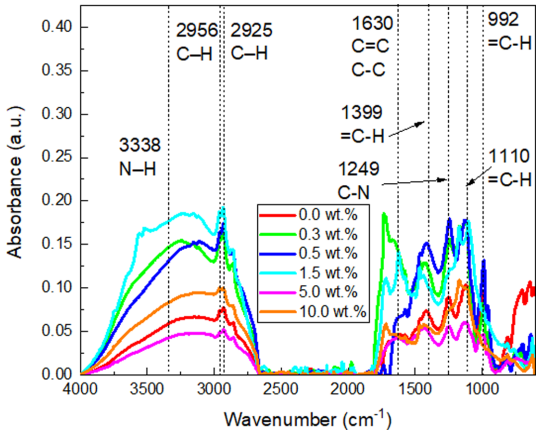

Fig. 3. FTIR absorbance profiles of PPy/FTO films synthesized with 0.0–10.0 wt.% water content.

successful polymerization and the linkage of pyrrole units via nitrogen atoms. Additionally, the peaks at 1399 cm^{-1} and 1110 cm^{-1} are associated with =C–H in-plane deformations, while the band at 992 cm^{-1} corresponds to out-of-plane =C–H wagging modes, both consistent with the planar geometry of the conjugated polypyrrole chain. These spectral features align well with those reported in the literature for polypyrrole, confirming the identity of the deposited material.[31,48–50)]

Beyond confirming the PPy structure, particular attention should be paid to specific spectral regions that can provide insights into the electronic properties of the synthesized films. In the 1000–1200 cm^{-1} region, specific vibrational modes are highly sensitive to the doping level of PPy.[51)] Within this spectral window, the integrated band area centered at 1110 cm^{-1} shows a systematic dependence on the water content used during synthesis. The signal increases progressively from the water-free sample (0.0 wt.%) to reach a maximum at 1.50 wt.%. Beyond this optimum, a pronounced decrease is observed at 5.00 wt.%, followed by a partial recovery at 10.00 wt.%. The observed trend suggests that a 1.50 wt.% water content promotes optimal doping and a more ordered polymer matrix. Conversely, excess water ($\geq$ 5.00 wt.%) likely introduces structural defects or chain disorder, thereby diminishing the intensity of these characteristic bands and indicating a less efficient doping process.

3.3 Nucleation and growth kinetics of PPy films

It is important to study the nucleation and growth mechanism of the film structure during modification. In the literature, the nucleation and growth mechanism for the electrodeposition of metals has been reported most often. The theory model for the nucleation and growth of metals was well developed. Thus, the mechanism of conducting polymer growth can be demonstrated using the theory model of metal growth.[24,28)] Unlike metals, PPy electrodeposition involves dynamically evolving electroactive areas and porous, anisotropic structures that violate assumptions of constant surface area.[52)] The process includes multiple simultaneous contributions rather than a single nucleation event.[53)] Thus, quantitative parameters should be interpreted with caution regarding the variable electroactive area.

Table 1. R^2 values from fitting chronoamperometric data to instantaneous and progressive 2D/3D nucleation models.

Film	2D inst	2D prog	3D inst	3D prog
0.0 wt.%	0.51136	0.37351	0.82519	0.88281
0.3 wt.%	0.53586	0.42518	0.82343	0.92452
0.5 wt.%	0.50901	0.41173	0.78358	0.91282
1.5 wt.%	0.50711	0.41517	0.77600	0.91221
5.0 wt.%	0.52862	0.38562	0.76514	0.87920
10.0 wt.%	0.35957	0.23424	0.65655	0.73046

The chronoamperometric behavior of PPy film formation on FTO substrates was analyzed by fitting the experimental current–time transients to theoretical models for instantaneous and progressive nucleation under both two-dimensional (2D) and three-dimensional (3D) growth regimes, as illustrated in Fig. 4. The corresponding R^2 values are summarized in Table 1. A clear trend emerges: for all water contents tested, the highest R^2 values consistently correspond to the progressive 3D nucleation model. In contrast, the fits to 2D models significantly lower R^2 values, never exceeding 0.55. This indicates that the electrochemical deposition of PPy on FTO is best described by a mechanism involving progressive nucleation and 3D growth.

The 3D progressive growth observed in all PPy films deposited originates from the combined influence of interfacial energetics and the substrate´s surface topography. The weak chemical interaction between PPy and FTO results in low adhesive forces relative to the cohesive forces within the polymer, creating a thermodynamic driving force for the deposit to minimize contact with the substrate by forming isolated three-dimensional islands.[54,55)] Moreover, FTO's rough and defective surface provides a heterogeneous landscape rich in preferential nucleation sites.[56–59)] These defects do not activate simultaneously; instead, they become electrochemically active gradually over time, leading to the continuous emergence of new nuclei during the early stages of deposition. Thus, the 3D progressive growth mode is a direct consequence of the FTO

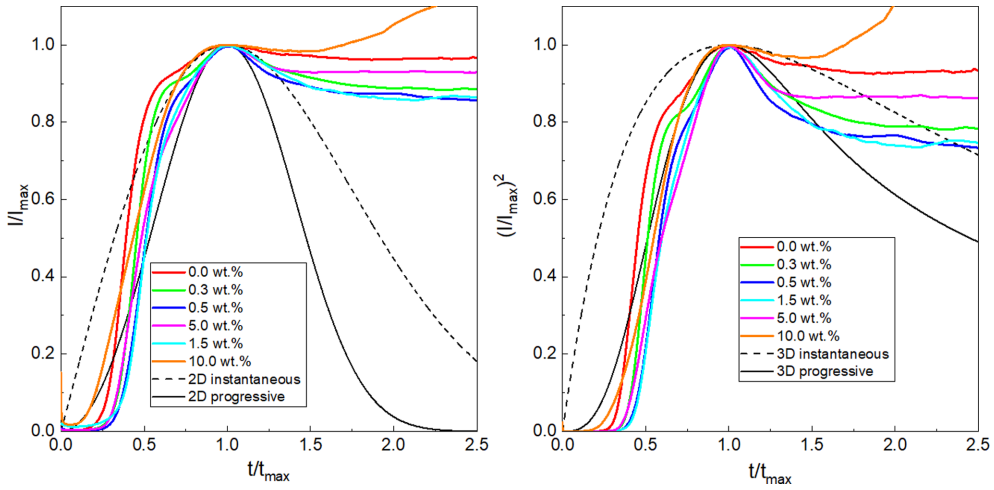

Fig. 4. Chronoamperometric analysis of PPy film formation: fitting to instantaneous and progressive 2D and 3D nucleation models.

substrate's physical characteristics. Thus, the substrate's microstructure plays a decisive role in dictating the nucleation mechanism, favoring progressive 3D growth even under varying synthesis conditions. These findings underscore that water does not alter the nucleation mode.

3.4 Influence of controlled rate addition on sheet resistance and bulk conductivity

3.4.1 Sheet resistance (Rs)

The sheet resistance (Rs) of electrosynthesized PPy films on FTO substrates exhibits a pronounced dependence on the water content in the polymerization electrolyte, as illustrated in Fig. 5. A sharp decrease in Rs is observed upon introduction of even small amounts of water: from 433.11 Ω/sq for the film deposited without water (0.0 wt.%), to 272.86 Ω/sq at 0.3 wt.% and 235.15 Ω/sq at 1.5 wt.%. This trend suggests that water plays a critical role in enhancing the in-plane conductivity of PPy during its formation. Notably, the lowest sheet resistance (131 Ω/sq) is achieved at 10.0 wt.% water content, representing a reduction of over 70% compared to the dry condition.

These results stand in stark contrast to the well-documented limitations of using water as the primary solvent, which typically yields poorly conducting and electrochemically inefficient PPy. As demonstrated by Yan et al., PPy synthesized in

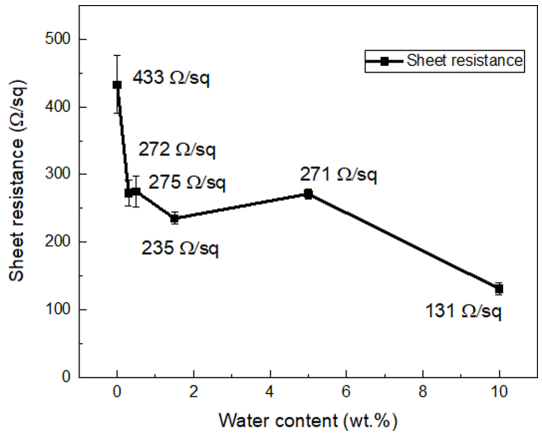

Fig. 5. Sheet resistance (Rs) of PPy films as a function of water content in the polymerization electrolyte.

water exhibits the lowest conductivity among common solvents such as acetonitrile or nitromethane, highlighting that while water enables electropolymerization, it is suboptimal for achieving high electronic performance in PPy.[22] This conclusion is strongly supported by Istakova et al., who quantified the extremely low electrochemical efficiency of PPy synthesis in pure water using chronoamperometry. They reported that over 99% of the charge passed during polymerization does not yield electroactive material, effectively confirming that aqueous media fail to produce functional conducting polymer

under these conditions.[60] Another explanation for the detrimental role of water lies in its strong solvating power toward small cations.[61] As demonstrated by Dorn et al., ions with small ionic radii, such as lithium, are extensively surrounded by water molecules, forming a bulky solvation shell that increases their effective radius. This solvation reduces ionic mobility, thereby impairing charge transport and negatively affecting the electrical conductivity of the electrolyte solution during polymerization.[62] Conversely, in the less polar ACN medium, the solvation shell is less voluminous, allowing for higher intrinsic ion mobility despite the potential for partial dissociation behavior characteristic of less polar solvents.[63]

Despite these detrimental effects when used as a solvent, water plays a fundamentally different and beneficial role when employed as an additive in non-aqueous electrolytes. First, as previously discussed, it mitigates local acidification at the electrode–solution interface. This suppresses defect-forming side reactions, enabling the growth of a more ordered polymer backbone with extended π-conjugation.[9] Second, water enhances the ionic conductivity of the supporting electrolyte. Its high dielectric constant (ε = 78.35 vs. 35.9 for ACN) promotes more complete salt dissociation, increasing the concentration of free charge carriers and lowering solution resistance.[62] This effect is clearly evident in the chronoamperometric curves, where polymerization currents rise systematically with water content. Even small water concentrations (0.3–0.5 wt.%) produce a marked enhancement in current response, with the highest currents observed at 10 wt.% water content. This observation aligns with the findings of Carquigny et al., who reported that trace amounts of water in ACN solutions led to a significant increase in the oxidation current peak, which they directly attributed to improved electrolyte conductivity.[64] This enhancement in electrolyte conductivity directly affects the ohmic potential drop (iR drop) between the reference electrode and WE. As established by Anantharaj et al., low electrolytic conductivity is a primary driver of the iR drop, which lowers the effective interfacial potential below the applied value. By reducing solution resistance, water ensures that the WE experience a potential closer to the nominal applied value.[65] Consistent with this observation, Oliveira et al. demonstrated that the conductivity of PANI films is directly related to low iR drop values, and optimized electrolyte conditions enhance the overall film conductivity.[66] Collectively, these mechanisms, local proton mitigation and enhanced electrolyte conductivity, ensure that the applied potential effectively drives pyrrole oxidation and promotes efficient chain propagation.

However, beyond 10 wt.%, the same interactions that initially enhance polymerization kinetics could begin to trigger degradation mechanisms. At water concentrations above this limit, the electropolymerization environment may become more susceptible to oxidative side reactions. As water content increases, pyrrole radical cations generated during monomer oxidation are expected to interact more frequently with water molecules, leading to the formation of undesirable, electrochemically inactive products, such as carbonyl groups. These groups incorporate at the β-position of the pyrrole rings, disrupting the π-conjugated backbone and driving the polymer into an overoxidized, insulating state.[67,68] This mechanistic interpretation is corroborated by Debiemme-Chouvy and Tran, who identified a characteristic Raman band at 1715 cm^{-1}, which they assigned with confidence to β-carbonyl defects arising from oxidative degradation in the presence of water.[67] Furthermore, as the water content approaches and exceeds 50 wt.%, the acetonitrile–water system typically exhibits limited miscibility, which may lead to partial phase separation.[68] Collectively, these chemical and physical considerations suggest that the beneficial effects observed at lower water contents are likely to diminish beyond 10 wt.%, potentially leading to a gradual increase in Rs as the water content rises. This trend aligns with the previously discussed literature, which consistently shows that using pure water as the primary solvent negatively affects the electrical performance of PPy.[22,60–63]

3.4.2 Bulk conductivity (σ)

According to the results shown in Fig. 5. Sheet resistance (Rs) of PPy films as a function of water content in the polymerization electrolyte., sheet

resistance decreases with increasing water content, suggesting that bulk conductivity should increase. However, the opposite behavior was observed in Fig. 6: bulk conductivity decreased with increasing the water content above 0.3 wt.%, indicating a contrasting relationship between the two electrical properties. To interpret this non-parallel response, it is essential to examine the microstructural architecture of the conducting polymer.

Conducting polymers possess a semi-crystalline microstructure where charge transport is inherently anisotropic. While intrachain conduction along conjugated backbones is highly efficient and interchain hopping between π-stacked chains is moderate, lateral charge transfer across the wider intercolumnar spacing is severely hindered by amorphous domains and dopant-mediated gaps. This directional dependence makes the macroscopic orientation of polymer crystallites relative to the substrate a decisive factor in determining overall electrical performance.[33,34,69–72] Guided by this principle, the divergent electrical trends observed in our PPy/FTO films can be rationalized through a specific molecu-

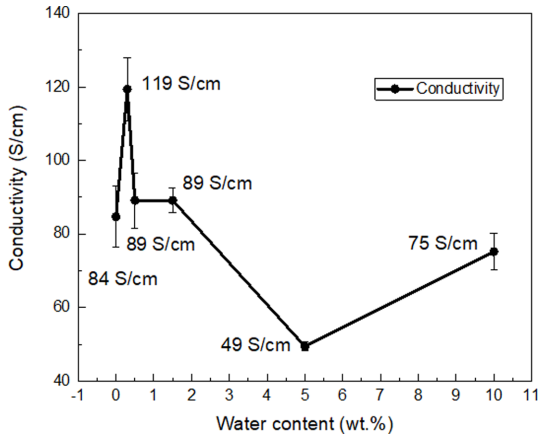

Fig. 6. Bulk conductivity (σ) of PPy films as a function of water content in the polymerization electrolyte.

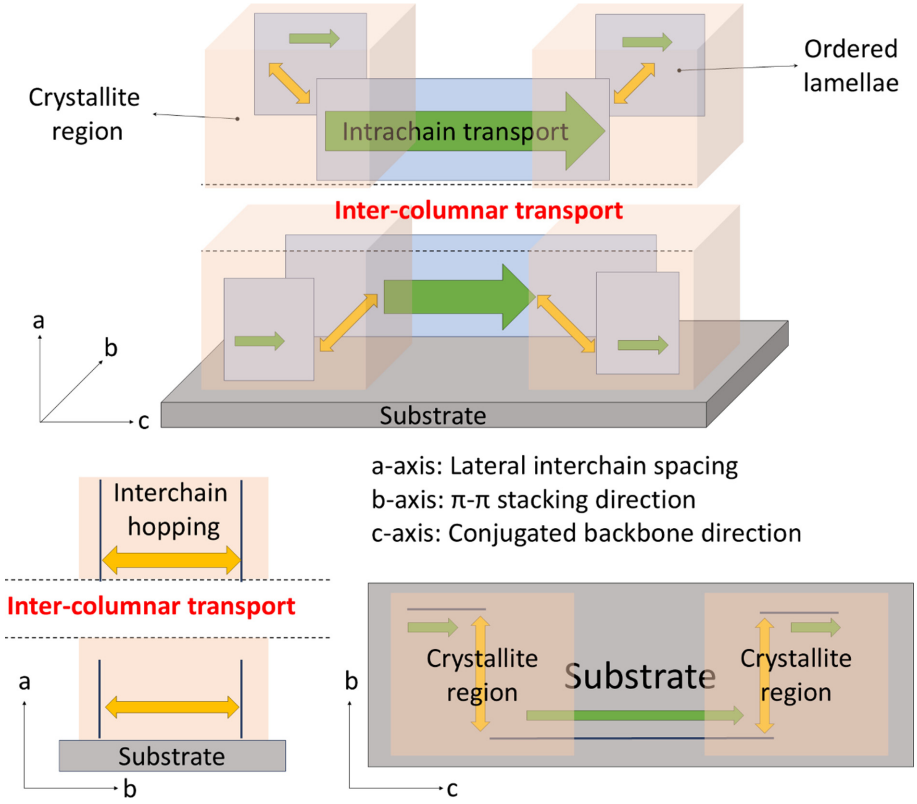

Fig. 7. Schematic representation of possible current transport in edge-on oriented PPy films.

lar packing arrangement. Consistent with this framework, the experimental data suggest that the film adopts a predominant edge-on texture, in which both the conjugated backbone and π-π stacking are aligned parallel to the substrate while the lateral interchain spacing is oriented perpendicular to it (Fig. 7).[34,71] This structural arrangement provides a coherent framework for interpreting the divergent electrical trends observed with increasing water content. Because the conjugated pathways and π-stacking planes lie parallel to the FTO surface, in-plane charge transport is highly efficient, which directly accounts for the continuous reduction in Rs across the entire 0.0–10.0 wt.% water range. In contrast, volumetric conduction requires carriers to repeatedly hop across the wider, less-ordered intercolumnar gaps that are oriented perpendicular to the substrate. This through-thickness charge transfer acts as the primary kinetic bottleneck, explaining why bulk conductivity (σ) does not scale proportionally with Rs.

This characteristic suggests a tunable approach to aligning electrical performance with the operational requirements of specific device architectures. Accordingly, for applications that depend on lateral charge transport across the film, such as solar cells or resistive gas sensors, sheet resistance (Rs) is the critical metric.[73,74] Specifically, for ammonia gas sensors, where Rs directly influences the detectability of resistance changes upon gas exposure, higher water contents (≥ 5 wt.%) may be advantageous for achieving high sensitivity and enabling fast response times.[73] Conversely, for applications requiring three-dimensional charge transport throughout the material, such as supercapacitors, batteries, and thermoelectric devices, minimal water addition (0.3 wt.%) appears more suitable for optimizing intrinsic bulk conductivity.[75,76] Taken together, these findings provide a practical framework to guide future material optimization for prospective sensor, energy conversion, and storage applications.

In summary, the systematic investigation of both sheet resistance (Rs) and bulk conductivity (σ) as a function of water content provides comprehensive experimental evidence that water significantly enhances the electrical performance of electrosynthesized PPy films through multiple mechanisms. This enhancement stems from water's dual role as a proton scavenger, which minimizes structural defects, and as an electrolyte, which enhances conductivity and reduces iR drop during polymerization. These findings underscore the importance of carefully tuning the water concentration in non-aqueous electropolymerization systems to achieve conductive polymers with tailored electronic properties for applications in flexible electronics, sensors, and energy storage devices.

4. Conclusion

This study demonstrates that water, when used as a controlled additive in acetonitrile-based electropolymerization, is not a contaminant but a strategic molecular regulator that significantly enhances the electrical performance of PPy films. The systematic increase in water content (0.0–10.0 wt.%) leads to a decrease in sheet resistance (from 433 to 131 Ω/sq, representing a > 70% reduction), while bulk conductivity exhibits a maximum of 120 S/cm at 0.3 wt.% water content followed by a decreasing trend, revealing a fundamental decoupling between in-plane and volumetric charge transport. This enhancement in Rs arises from the suppression of proton-driven side reactions that generate structural defects, thereby preserving extended conjugation length along the polymer backbone. The divergent behavior is consistent with a predominant edge-on texture, in which both conjugated backbones and π-π stacking align parallel to the substrate, enabling efficient in-plane charge transport that continuously reduces Rs. However, bulk conductivity is fundamentally constrained by charge transfer across the lateral interchain spacing, which is oriented perpendicular to the substrate, acting as the kinetic bottleneck for three-dimensional conduction. At 0.3 wt.% water content, optimal bulk conductivity results from the dual effect of extended conjugation length and minimized intercolumnar spacing. Crucially, this optimization occurs without modifying the fundamental progressive 3D nucleation mechanism on FTO, underscoring that water acts at the molecular level rather than altering growth kinetics.

The results further highlight the context-dependent nature of water’s influence: while it degrades PPy

conductivity when used as the primary solvent due to its high donor number and nucleophilic interference with radical intermediates, it becomes highly beneficial as a trace additive in aprotic media by mitigating interfacial acidification. This duality emphasizes that the role of water must be evaluated in terms of concentration and chemical environment.

References

1. M. B. Hasan, M. M. Parvez, A. Y. Abir, and M. F. Ahmad, A review on conducting organic polymers: concepts, applications, and potential environmental benefits, *Heliyon*, **11(3)**, e42375 (2025).
2. M. G. Tadesse, A. S. Ahmmed, and J. F. Lübben, Review on conductive polymer composites for supercapacitor applications, *J. Compos. Sci.*, **8(2)**, 53 (2024).
3. S. M. Merdas, A. K. Zaid, and Z. M. Kareem, Conducting polymers and their applications in sensors: a review, *J. Educ. Pure Sci. - Univ. Thi-Qar*, **11(1)**, 22–32 (2021).
4. M. I. Pilo, G. Sanna, and N. Spano, Conducting polymers in amperometric sensors: A state of the art over the last 15 years with a focus on polypyrrole-, polythiophene-, and poly(3,4-ethylenedioxythiophene)-based materials, *Chemosensors*, **12(5)**, 81 (2024).
5. H. Ding, A. M. Hussein, I. Ahmad, R. Latef, J. K. Abbas, A. T. A. Ali, S. M. Saeed, A. S. Abdulwahid, M. F. Ramadan, H. A. Rasool, and A. Elawady, Conducting polymers in industry: a comprehensive review on the characterization, synthesis and application, *Alex. Eng. J.*, **88(1)**, 253–267 (2024).
6. H. Song, T. Li, Y. Han, Y. Wang, C. Zhang, and Q. Wang, Optimizing the polymerization conditions of conductive polypyrrole, *J. Photopolym. Sci. Technol.*, **29(6)**, 803–808 (2016).
7. I. Sapurina, Y. Li, E. Alekseeva, P. Bober, M. Trchová, Z. Morávková, and J. Stejskal, Polypyrrole nanotubes: the tuning of morphology and conductivity, *Polymer,* **113(1)**, 247–258 (2017).
8. P. Bober, Y. Li, U. Acharya, Y. Panthi, J. Pfleger, P. Humpolíček, M. Trchová, and J. Stejskal, Acid blue dyes in polypyrrole synthesis: the control of polymer morphology at nanoscale in the promotion of high conductivity and the reduction of cytotoxicity, *Synth. Met.*, **237(1)**, 40–49 (2018).
9. S. Sadki, P. Schottland, G. Sabouraud, and N. Brodie, The mechanisms of pyrrole electropolymerization, *Chem. Soc. Rev.*, **29(5)**, 283–293 (2000).
10. S. Majumdar, K. Sarmah, and D. Mahanta, A simple route to prepare polypyrrole-coated filter papers via vapor phase polymerization and their gas sensing application, *ACS Appl. Polym. Mater.*, **2(5)**, 1933–1942 (2020).
11. L. Hao, C. Dong, and D. Yu, Polypyrrole derivatives: preparation, properties and application, *Polymers*, **16(16)**, 2233 (2024).
12. A. K. Sarangi, L. Tripathy, A. Ansari, R. K. Mohapatra, and S. K. Bhoi, Enhancing conductivity in polymers: the role of metal ions in conducting polymer systems, *Polym. Adv. Technol.,* **35(7)**, e6505 (2024).
13. J. Stejskal, M. Trchová, P. Bober, Z. Morávková, D. Kopecký, M. Vrňata, J. Prokeš, M. Varga, and E. Watzlová, Polypyrrole salts and bases: superior conductivity of nanotubes and their stability towards the loss of conductivity by deprotonation, *RSC Adv.*, **6(91)**, 88382–88391 (2016).
14. F. Khadem, M. Pishvaei, M. Salami-Kalajahi, and F. Najafi, Morphology control of conducting polypyrrole nanostructures via operational conditions in the emulsion polymerization, *J. Appl. Polym. Sci.*, **134(15)**, 44697 (2017).
15. Y. Li, P. Bober, M. Trchová, and J. Stejskal, Polypyrrole prepared in the presence of methyl orange and ethyl orange: nanotubes versus globules in conductivity enhancement, *J. Mater. Chem. C*, **5(17)**, 4236–4245 (2017).
16. J. Deng, X. Wang, J. Guo, and P. Liu, Effect of the oxidant/monomer ratio and the washing post-treatment on electrochemical properties of conductive polymers, *Ind. Eng. Chem. Res.*, **53(35)**, 13680–13689 (2014).
17. M. Li, W. Li, J. Liu, and J. Yao, Preparation and characterization of PPy doped with different anionic surfactants, *Polym. Eng. Sci.*, **53(11)**, 2465–2469 (2013).
18. O. Y. Posudievsky and O. A. Kozarenko, Effect of monomer/oxidant mole ratio on polymerization mechanism, conductivity and spectral characteristics of mechanochemically prepared polypyrrole, *Polym. Chem.*, **2(1)**, 216–220 (2011).
19. L. Fang, L. Zhao, X. Liang, H. Xiao, and L. Qian, Effects of oxidant and dopants on the properties of cellulose/PPy conductive composite hydrogels, *J. Appl. Polym. Sci.*, **133(34)**, 43759 (2016).
20. A. Yussuf, M. Al-Saleh, S. Al-Enezi, and G. Abraham, Synthesis and characterization of conductive polypyrrole: the influence of the oxidants and monomer on the electrical, thermal, and morphological properties, *Int. J. Polym. Sci.*, **2018(1)**, 4191747 (2018).
21. M. Varga, J. Kopecká, Z. Morávková, I. Křivka, M. Trchová, J. Stejskal, and J. Prokeš, Effect of oxidant on electronic transport in polypyrrole nanotubes synthesized in the presence of methyl orange, *J. Polym. Sci. B Polym. Phys.*, **53(16)**, 1147–1159 (2015).
22. Q. Yan, W. Pan, S. Zhong, R. Zhu, and G. Li, Effect of solvents on the preparation and corrosion protection of polypyrrole, *Prog. Org. Coat.*, **132(1)**, 298–304 (2019).
23. M. Zhou and J. Heinze, Electropolymerization of pyrrole and electrochemical study of polypyrrole. 3. nature of 'water effect' in acetonitrile, *J. Phys. Chem. B*, **103(40)**, 8451–8457 (1999).

24. B.-J. Hwang, R. Santhanam, and Y.-L. Lin, Evaluation of structure, nucleation and growth mechanism of electropolymerized polypyrrole on highly oriented pyrolytic graphite electrode, *Electroanalysis*, **15(2)**, 115–120 (2003).
25. J. Puerres, P. Ortiz, and María T. Cortés, Effect of electrosynthesis potential on nucleation, growth, adhesion, and electronic properties of polypyrrole thin films on Fluorine-doped Tin Oxide (FTO), *Polymers*, **13(15)**, 2419 (2021).
26. A. Castro-Beltran, C. Dominguez, D. Bahena-Uribe, S. Sepulveda-Guzman, and R. Cruz-Silva, Effect of non-electroactive additives on the early stage pyrrole electropolymerization on indium tin oxide electrodes, *Thin Solid Films*, **566(1)**, 23–31 (2014).
27. Y. Wang and D. O. Northwood, An investigation into the nucleation and growth of an electropolymerized polypyrrole coating on a 316L stainless steel surface, *Thin Solid Films*, **516(21)**, 7427–7432 (2008).
28. B. J. Hwang, R. Santhanam, and Y. L. Lin, Nucleation and growth mechanism of electroformation of polypyrrole on a heat-treated gold/highly oriented pyrolytic graphite, *Electrochim. Acta*, **46(18)**, 2843–2853 (2001).
29. M. Madadelahi, F. O. Romero-Soto, R. Kumar, U. B. Tlaxcala, and M. J. Madou, Electrochemical sensors: types, applications, and the novel impacts of vibration and fluid flow for microfluidic integration, *Biosens. Bioelectron.*, **272(1)**, 117166 (2025).
30. I. Sadriu, S. Bouden, J. Nicolle, F. I. Podvorica, V. Bertagna, C. Berho, L. Amalric, and C. Vautrin-Ul, Molecularly imprinted polymer modified glassy carbon electrodes for the electrochemical analysis of isoproturon in water, *Talanta*, **207(1)**, 120222 (2020).
31. M. A. Chougule, S. G. Pawar, P. R. Godse, R. N. Mulik, S. Sen, and V. B. Patil, Synthesis and characterization of polypyrrole (PPy) thin films, *Soft Nanosci. Lett.*, **2011(1)**, 6–10 (2011).
32. Z. Cui, C. Coletta, A. Dazzi, P. Lefrançois, M. Gervais, S. Néron, and S. Remita, Radiolytic method as a novel approach for the synthesis of nanostructured conducting polypyrrole, *Langmuir*, **30(46)**, 14086–14094 (2014).
33. M. Heydari Gharahcheshmeh and K. Chowdhury, Fabrication methods, pseudocapacitance characteristics, and integration of conjugated conducting polymers in electrochemical energy storage devices, *Energy Adv.*, **3(11)**, 2668–2703 (2024).
34. S. H. K. Paleti, Y. Kim, J. Kimpel, M. Craighero, S. Haraguchi, and C. Müller, Impact of doping on the mechanical properties of conjugated polymers, *Chem. Soc. Rev.*, **53(4)**, 1702–1729 (2024).
35. M. A. del Valle, M. A. Gacitúa, F. Hernández, M. Luengo, and L. A. Hernández, Nanostructured conducting polymers and their applications in energy storage devices, *Polymers*, **15(6)**, 1450 (2023).
36. A. L. Pang, A. Arsad, and M. Ahmadipour, Synthesis and factor affecting on the conductivity of polypyrrole: a short review, *Polym. Adv. Technol.*, **32(4)**, 1428–1454 (2021).
37. Y. Tan and K. Ghandi, Kinetics and mechanism of pyrrole chemical polymerization, *Synth. Met.*, **175(1)**, 183–191 (2013).
38. A. J. Bard and L. R. Faulkner, *Electrochemical Methods: Fundamentals and Applications*, 2nd ed., John Wiley & Sons, New York (2001).
39. T. Di Giulio, I. M. Asif, M. Corsi, S. Rajpal, B. Mizaikoff, N. Ditaranto, G. E. De Benedetto, C. Malitesta, G. Barillaro, and E. Mazzotta, A molecularly imprinted polymer-based porous silicon optical sensor for quercetin detection in wines, *ACS Appl. Mater. Interfaces*, **17(8)**, 12663–12675 (2025).
40. R. J. Mayer, N. Hampel, and A. R. Ofial, Lewis acidic boranes, Lewis bases, and equilibrium constants: a reliable scaffold for a quantitative Lewis acidity/basicity scale, *Chem. Eur. J.*, **27(12)**, 4070–4080 (2021).
41. B. S. Bahl and A. Bahl, *Advanced Organic Chemistry*, 1st ed., S. Chand & Co. Ltd., New Delhi (1977).
42. G. Jahnavi, K. Chandrasekhar, B. V. Ramana, and K. V. S. Reddy, A review article on biological importance of pyrrole, *World J. Pharm. Res.*, **12(7)**, 995–1021 (2023).
43. R. Chang, *Química*, 10th ed., McGraw-Hill Interamericana Editores, Mexico City (2010).
44. H. Khatoon and S. Ahmad, Vanadium pentoxide-enwrapped polydiphenylamine/polyurethane nanocomposite: high-performance anticorrosive coating, *ACS Appl. Mater. Interfaces*, **11(2)**, 2374–2385 (2019).
45. O. Folorunso, N. Kumar, Y. Hamam, R. Sadiku, and S. S. Ray, Facile solvent/drying fabrication of PVA/PPy/rGO: a novel nanocomposite for energy storage applications, *Results Mater.*, **15(1)**, 100295 (2022).
46. D. C. Lingegowda, J. Komal Kumar, A. G. Devi Prasad, M. Zarei, and S. Gopal, FTIR spectroscopic studies on cleome gynandra-comparative analysis of functional group before and after extraction, *Rom. J. Biophys.*, **22(3–4)**, 137–143 (2012).
47. W. Zhao, Y. Wang, and A. Wang, Nonlinear optical properties of novel polypyrrole derivatives bearing different aromatic segments, *Mater. Sci. Appl.*, **8(11)**, 774–783 (2017).
48. Y. Fu and A. Manthiram, Core-shell structured sulfur-polypyrrole composite cathodes for lithium-sulfur batteries, *RSC Adv.*, **2(14)**, 5927–5929 (2012).
49. B. H. Taymaz, H. Kamiş, and Ö. Yoldaş, Photocatalytic degradation of malachite green dye using zero valent iron doped polypyrrole, *Environ. Eng. Res.*, **27(2)**, 200638 (2022).
50. O. Gürbüz, B. F. Şenkal, and O. İçelli, Structural, optical and electrical properties of polypyrrole in an ionic liquid, *Polym. Bull.*, **74(7)**, 2625–2639 (2017).
51. J. Hazarika and A. Kumar, Studies of structural, optical, dielectric relaxation and ac conductivity of different alkylbenzenesulfonic acids doped polypyrrole nanofibers, *Phys. B: Condens. Matter*, **481(1)**, 268–279 (2016).

52. W. Kim, S. Cho, and J. S. Lee, Comparative study on the effect of protonation control for resistive gas sensor based on close-packed polypyrrole nanoparticles, *Appl. Sci.,* **10(5)**, 1850 (2020).
53. T.-X. Chu, Nucleation in polymer. In: M. E. Palomar-Pardavé and T. L. Manh (eds.), *Nucleation and Growth in Applied Materials*, pp. 203–228, Elsevier (2024).
54. H. Z. Yu and C. V. Thompson, Grain growth and complex stress evolution during volmer-weber growth of polycrystalline thin films, *Acta Mater.*, **67(1)**, 189–198 (2014).
55. Y. Wan, W. Qiu, H. Zhu, Q. Zhang, and S. Zhu, Engineering cohesion and adhesion through dynamic bonds for advanced adhesive materials, *Can. J. Chem. Eng.*, **101(9)**, 4941–4954 (2023).
56. R. Ramírez-Amador, J. J. Alvarado-Pulido, H. P. Martínez-Hernández, R. Cortes-Maldonado, S. Alcántara-Iniesta, G. Flores-Carrasco, E. Ojeda-Durán, O. Malik, L. Morales-de la Garza, and M. Á. Méndez-Rojas, Study of fluorine-doped tin oxide thin films deposited by pneumatic spray pyrolysis and ultrasonic spray pyrolysis: a direct comparison, *Mater. Res. Express*, **10(6)**, 066402 (2023).
57. L. T. C. Tuyen, S. R. Jian, N. T. Tien, and P. H. Le, Nanomechanical and material properties of fluorine-doped tin oxide thin films prepared by ultrasonic spray pyrolysis: effects of F-doping, *Materials*, **12(10)**, 1665 (2019).
58. S. L. Triana, Kusumandari, and R. Suryana, Effect of wet etching process on the morphology and transmittance of fluorine doped tin oxide (FTO), *J. Phys. Conf. Ser.*, **776(1)**, 012005 (2016).
59. J. W. Bae, B. R. Koo, H. R. An, and H. J. Ahn, Surface modification of fluorine-doped tin oxide films using electrochemical etching for dye-sensitized solar cells, *Ceram. Int.*, **41(10)**, 14668–14673 (2015).
60. O. I. Istakova, D. V. Konev, T. O. Medvedeva, E. V. Zolotukhina, and M. A. Vorotyntsev, Efficiency of pyrrole electropolymerization under various conditions, *Russ. J. Electrochem.*, **54(12)**, 1243–1251 (2018).
61. V. V. Shcherbakov, Y. M. Artemkina, I. A. Akimova, and I. M. Artemkina, Dielectric characteristics, electrical conductivity and solvation of ions in electrolyte solutions, *Materials*, **14(19)**, 5617 (2021).
62. M. Dorn, S. Kareth, E. Weidner, and M. Petermann, Electrical conductivity of lithium, sodium, potassium, and quaternary ammonium salts in water, acetonitrile, methanol, and ethanol over a wide concentration range, *J. Chem. Eng. Data*, **69(4)**, 1493–1502 (2024).
63. H. Hanibah, N. Z. N. Hashim, and I. J. Shamsudin, Molar conductivity behavior of ionic liquid compare to inorganic salt in electrolyte solution at ambient temperature, *AIP Conf. Proc.*, **1877(1)**, 050003 (2017).
64. S. Carquigny, O. Segut, B. Lakard, F. Lallemand, and P. Fievet, Effect of electrolyte solvent on the morphology of polypyrrole films: application to the use of polypyrrole in pH sensors, *Synth. Met.*, **158(11)**, 453–461 (2008).
65. S. Anantharaj and S. Noda, iR drop correction in electrocatalysis: everything one needs to know!, *J. Mater. Chem. A*, **10(17)**, 9348–9354 (2022).
66. R. D. Oliveira, C. S. Santos, J. R. Garcia, M. Vidotti, L. F. Marchesi, and C. A. Pessoa, IR drop studies of poly(aniline)-based modified electrodes, *J. Electroanal. Chem.*, **878(1)**, 114662 (2020).
67. C. Debiemme-Chouvy and T. T. M. Tran, An insight into the overoxidation of polypyrrole materials, *Electrochem. Commun.*, **10(6)**, 947–950 (2008).
68. C.-Y. Lau, J. Xu, and K.-K. Shiu, Effects of solvent composition on the preparation and electroanalytical behaviors of polypyrrole modified electrodes, *Electrochim. Acta*, **72(1)**, 143–149 (2012).
69. A. Nijkoops, M. Ciocca, M. A. C. Angeli, M. Ahmad, R. Boom, N. Münzenrieder, P. Lugli, and L. Petti, Recent advances in conducting polymer chemiresistive sensors for ammonia gas detection: materials, characterization, and applications, *J. Phys. Mater.*, **9(1)**, 012002 (2025).
70. M. H. Gharahcheshmeh and K. K. Gleason, Texture and nanostructural engineering of conjugated conducting and semiconducting polymers, *Mater. Today Adv.*, **8(1)**, 100086 (2020).
71. M. H. Gharahcheshmeh and K. K. Gleason, Recent progress in conjugated conducting and semiconducting polymers for energy devices, *Energies*, **15(10)**, 3661 (2022).
72. M. H. Gharahcheshmeh and K. K. Gleason, Device fabrication based on oxidative chemical vapor deposition (oCVD) synthesis of conducting polymers and related conjugated organic materials, *Adv. Mater. Interfaces*, **6(1)**, 1801564 (2019).
73. R. Kumar, A. Kumar, R. Singh, R. Kashyap, D. Kumar, R. Goel, and M. Kumar, Investigation of sheet resistance variation with annealing temperature and development of highly sensitive and selective room temperature ammonia gas sensor using functionalized graphene oxide, *J. Mater. Sci.: Mater. Electron.*, **32(2)**, 1716–1728 (2021).
74. Y. Zhang, S.-W. Ng, X. Lu, and Z. Zheng, Solution-processed transparent electrodes for emerging thin-film solar cells, *Chem. Rev.*, **120(4)**, 2049–2122 (2020).
75. R. Xiao, X. Zhou, C. Zhang, X. Liu, S. Han, and C. Che, Organic thermoelectric materials for wearable electronic devices, *Sensors*, **24(14)**, 4600 (2024).
76. G. J. Adekoya, O. C. Adekoya, R. E. Sadiku, Y. Hamam, and S. S. Ray, Applications of MXene-containing polypyrrole nanocomposites in electrochemical energy storage and conversion, *ACS Omega*, **7(44)**, 39498–39519 (2022).